frontiers | Frontiers in Nuclear Engineering

TYPE Original Research
PUBLISHED 10 February 2025
DOI 10.3389/fnuen.2025.1534820

OPEN ACCESS

EDITED BY
Danny J. Edwards,
Pacific Northwest National Laboratory (DOE), United States

REVIEWED BY
Mukesh Bachhav,
Idaho National Laboratory (DOE), United States
Sourabh Bhagwan Kadambi,
Idaho National Laboratory (DOE), United States

*CORRESPONDENCE
Alex Leide,
alex.leide@ukaea.uk

RECEIVED 26 November 2024
ACCEPTED 10 January 2025
PUBLISHED 10 February 2025

CITATION
Leide A, Zhong W, Fernandez-Victorio I, Nguyen-Manh D and Koyanagi T (2025) Effect of microstructure and neutron irradiation defects on deuterium retention in SiC. *Front. Nucl. Eng.* 4:1534820. doi: 10.3389/fnuen.2025.1534820

Effect of microstructure and neutron irradiation defects on deuterium retention in SiC

Alex Leide[1]*, Weicheng Zhong[2], Isabel Fernandez-Victorio[1,3], Duc Nguyen-Manh[1,3] and Takaaki Koyanagi[2]

[1]Materials Division, United Kingdom Atomic Energy Authority, Abingdon, United Kingdom, [2]Materials Science and Technology Division, Oak Ridge National Laboratory, Oak Ridge, TN, United States, [3]Department of Materials, University of Oxford, Oxford, United Kingdom

Retention of hydrogen isotopes is a critical concern for operating fusion reactors as retained tritium both activates components and removes scarce fuel from the fuel cycle. Radiation-induced displacement damage in SiC influences the retention of hydrogen isotopes compared to pristine SiC. Deuterium retention in neutron irradiated high purity SiC has been compared to different microstructures of non-irradiated high purity SiC using thermal desorption spectroscopy after gas charging and low energy ion implantation. Experimental results show lower deuterium retention in single crystal SiC than in polycrystal SiC indicating that grain boundaries are key trapping features in unirradiated SiC. Deuterium is released at lower temperatures in neutron irradiated polycrystal SiC compared to pristine polycrystal SiC, suggesting weaker trapping by radiation-induced defects compared to grain boundary trapping sites in the pristine materials. Low energy ion implantation caused a high deuterium release temperature, highlighting the sensitivity of deuterium release behaviour to radiation defect characteristics. First principles calculations have been conducted to identify energetically favourable trapping sites in SiC at the $H_{ABc}V_{Si}$ and $H_{TSi}V_C$ complexes, and migration barriers between interstitial sites. This helps interpret experimental results and derive effective diffusivity of hydrogen isotopes in SiC in the presence of vacancies.

KEYWORDS

silicon carbide, hydrogen isotope retention, thermal desorption spectroscopy (TDS), neutron radiation damage, density function theory (DFT)

1 Introduction

Commercial fusion reactors are reliant on a hydrogen fuel cycle, along with the issues this poses around containing and transporting hydrogen including the radioactive tritium isotope and deuterium (Lord et al., 2024). Minimising tritium trapped in the reactor components is vital to ensure sufficient tritium is available in the fuel cycle, and to minimise the radioactivity of components caused by retained tritium (Tanabe, 2011). Therefore, an understanding of the retention behaviour of hydrogen isotopes is important for successful reactor operations.

Silicon carbide and its fibre reinforced composites can operate in radiation environments even at ~1,000°C, enabling the breeder blanket of a fusion reactor to generate useful process heat and utilise efficient thermodynamic electricity generating cycles (Koyanagi et al., 2018; Tillack et al., 2022; Pearson et al., 2022). As well as extracting energy, a fusion reactor breeder blanket must create tritium from the interaction of fusion

neutrons with lithium, which can be contained in the breeder blanket in a variety of forms including molten lithium, lead-lithium alloy, a molten salt such as FLiBe, or as a solid ceramic breeder (Lord et al., 2024; Federici et al., 2019; Konishi et al., 2017). The breeder material is one source of tritium generation within a blanket component from which it may enter a silicon carbide structural component via adsorption and diffusion.

A second source of hydrogen in SiC is by transmutation of silicon and carbon atoms. In particular, via the (n,p) reactions which have an energy threshold of 4 MeV for silicon and 13.6 MeV for carbon (Sawan et al., 2003). Although helium dominates the gaseous transmutation production via the (n,n'3α) reactions with carbon atoms, several thousand parts per million of hydrogen atoms will be generated internally from silicon (Sawan et al., 2013). The synergistic effects of transmutation defects with displacement damage and hydrogen isotopes are an ongoing area of research in fusion materials.

Although monolithic SiC is not commonly considered as a plasma facing component due to poor thermal shock resistance, it does have certain benefits for plasma-material interactions as low atomic mass elements radiate less heat when they contaminate the plasma, and sputtering yield is lower than graphite components (Dienst, 1991; Abrams et al., 2021). With further maturity of SiC fiber-reinforced SiC matrix (SiC_f/SiC) composites as a way to mitigate thermal shock-induced catastrophic failures, SiC plasma facing components are gaining renewed interest (Abrams et al., 2021). Hydrogen isotopes can be introduced to plasma facing components by direct ion implantation from the plasma, or by co-deposition of sputtered material which is transported around the tokamak's magnetic field. Thermodynamics and trapping mechanisms for tritium in plasma facing materials are vital to understand for the purposes of tritium accountancy and detritiation methods for handling and disposal (Widdowson et al., 2021).

Previous studies investigated deuterium retention in a range of SiC materials by low energy implantation with deuterium ions followed by thermal desorption spectroscopy (TDS) to measure the deuterium release rate as a function of temperature. Oya identified four peaks in the thermal desorption spectrum of deuterium implanted SiC, claiming the peak at 450 K corresponds to deuterium adsorbed on the surface, 650 K to interstitial deuterium, 800 K for Si-D trapped deuterium, and 1,000 K for C-D trapped deuterium (Oya et al., 2013). Sugiyama identified 3 different peaks in their deuterium desorption experiments and related these to deuterium trap energies by repeating TDS experiments at different heating rates (Sugiyama et al., 2002). These were at higher temperatures than found by Oya; attributing the 800 K peak to Si-D bond, and the 1,200 K peak to C-D bond with the 1,080 K peak related to C-D trapping in helium pre-implanted carbon-rich regions, i.e., a region with displacement defects.

TDS results also appear to be a function of the implantation temperature, energy, and fluence, with different researchers identifying different numbers of peaks, or desorption rate peaks at different temperatures, making interpretation and comparison very difficult (Sugiyama et al., 2002; Nobuta et al., 2015; Koller et al., 2019; Sánchez et al., 2016). The deuterium ion fluences typically used for experiments in the literature are vast; between 10^{21} and 10^{24} D/m^2 with energy between 0.5 and 50 keV (Oya et al., 2013; Nobuta et al., 2015; Koller et al., 2019; Sánchez et al., 2016; Oya et al., 2005; Oya et al., 2002). Such high fluences are used as most deuterium is spontaneously desorbed rather than being trapped, and these experiments are intended to saturate trapping sites ahead of the TDS measurements. However, ion implantation also causes atomic displacements which will alter the microstructure of the target material. The threshold displacement energy for carbon and silicon atoms is 21 eV and 35 eV respectively, far lower than the threshold displacement energy for tungsten (90 eV) which is what most experimental parameters are based on (Devanathan and Weber, 2000; Schwarz-Selinger, 2023). Koller et al. identified a fluence of ~5 × 10^{21} D/m^2 to achieve saturation of deuterium in SiC for their experiments, and used a fluence of 1 × 10^{24} D/m^2 for most of their experiments (Koller et al., 2019). SRIM estimates of the displacements per atom (dpa) for SiC predict >10 dpa to achieve the "saturation" fluence and that the majority of their experiments imparted 1,500 peak dpa to the specimens during ion implantation (Koller et al., 2019; Ziegler et al., 2010). Most deuterium implantations are conducted at room temperature where SiC is easily amorphized, with a critical temperature threshold between 300 K and 500 K depending on radiation type (Yuan and Hobbs, 2002; Snead and Zinkle, 1996; Boulle et al., 2017). Above the critical amorphisation temperature, neutron irradiation defects in SiC are strongly temperature dependent, with a decreasing defect density (related to swelling) with increasing irradiation temperature, saturating at less than ~2 dpa (Katoh et al., 2018). Considering the high implantation doses used in the literature and the displacement damage this creates, the measured deuterium trapping properties will be from a damaged microstructure rather than a pristine microstructure. The effect of helium pre-implantation was investigated by Sugiyama et al., finding higher trapping energies for C-D bonds and a fluence-dependent trapping energy for Si-D trap sites compared to deuterium implantation alone; however, having found that helium irradiation changes desorption behaviour, the effect of displacement defects was not evaluated (Sugiyama et al., 2002).

A significant knowledge gap is the interaction of hydrogen isotopes with carbon atoms in SiC through forming covalent hydrocarbon bonds. Under irradiation at elevated temperatures, displacement events form a wide range of crystallographic defects including vacancies and interstitials, plus anti-site defects (Li et al., 1998). In terms of interatomic bonds, these crystallographic defects correspond to the accumulation of chemical disorder by breaking heteronuclear Si-C bonds and forming homonuclear Si-Si and C-C bonds. These bonds are regularly observed in Raman spectroscopy measurements of irradiated SiC, and in first principles calculations of defects which identify carbon bonding signals as coming from carbon clusters or chains with both sp^2 and sp^3 bonding (Koyanagi, 2022; Chaâbane et al., 2012; Leide et al., 2019). This creates a complex variety of atomic environments and interatomic bonding states to which hydrogen isotopes can bond.

This study investigates the effect of microstructure on the retention of deuterium in high purity polycrystalline cubic SiC, and for the first time the impact of neutron irradiation-induced defects on deuterium retention. Comparative studies are made between deuterium gas charging, and low energy ion implantation. These experimental results are discussed and

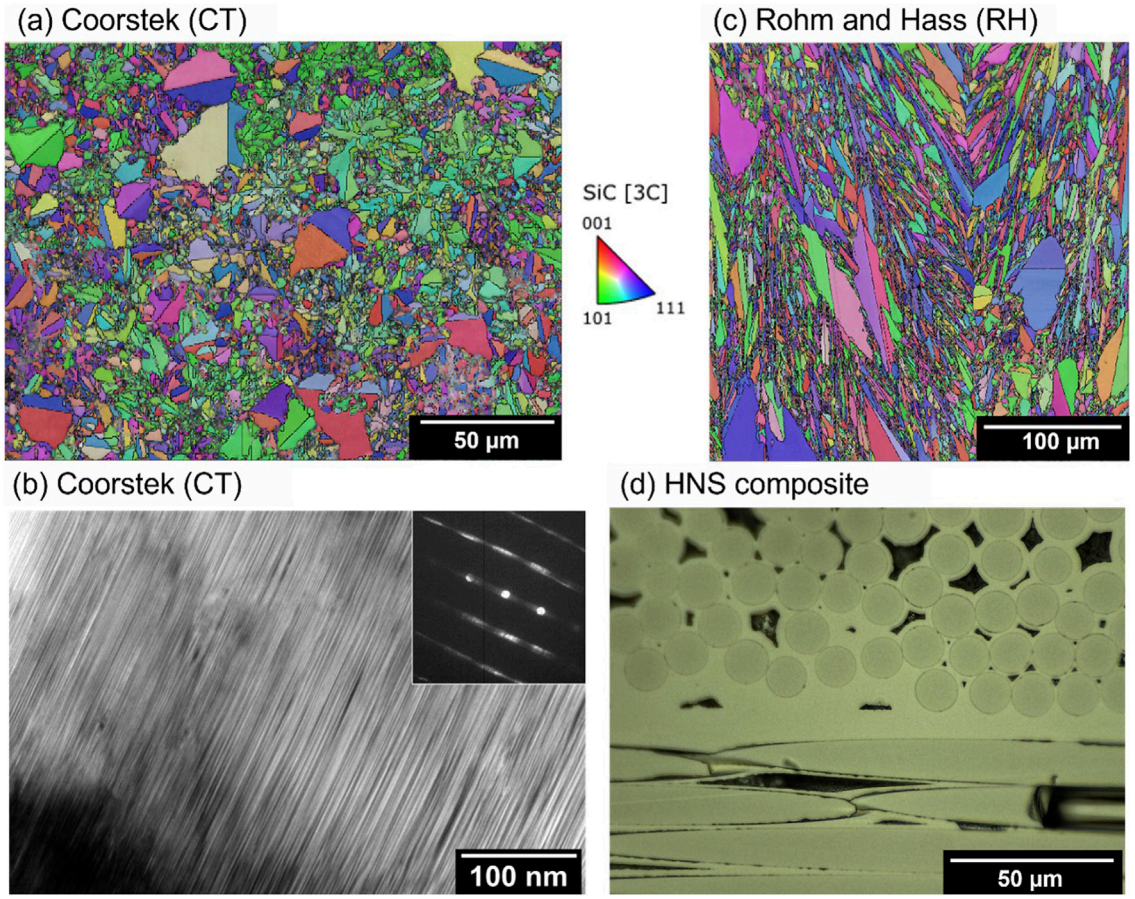

FIGURE 1
Microstructures of specimens studied in this work. **(A)** and **(C)** EBSD orientation maps of CT and RH CVD SiC samples. **(B)** TEM image of CT showing high stacking fault density. **(D)** Representative optical micrograph of HNS SiC_f/SiC composite.

interpreted in relation with the binding energies of hydrogen in vacancies obtained from first principles calculations. This is a step towards understanding the transport of hydrogen isotopes in SiC components of a fusion power station.

2 Experimental

2.1 Materials

Different grades of SiC were studied to investigate the effects of as-fabricated microstructure on deuterium retention. A high-resistivity grade 4H single crystal SiC was obtained from MSE Supplies LLC. The nominal impurities included 15 appm Al, 13 appm Fe, 28 appm Zn, and 15 appm K. The primary surface was parallel to the (0001) plane. Two types of polycrystalline chemical vapor deposited (CVD) 3C-SiC material were also tested; high-resistivity grade from Coorstek (CT) contained a high density of stacking faults and a mean grain size of 8 µm, and a specimen of from Rohm and Haas (RH) with a lower density of stacking faults and a 12 µm average grain size. Both samples have a range of grain sizes: RH appears to have a wider grain size distribution compared to CT with a larger "coarse" grain size, and smaller "fine" grain size. EBSD images of the CVD materials are shown in Figure 1 to demonstrate the differences in microstructure, along with a TEM image showing the high stacking fault density in CT. Both materials had nominal metallic purity above 99.9995% based on the vendor's material data sheet. Non-metallic impurities of N and O were determined by secondary ion mass spectrometry at Eurofins EAG Materials Science, LLC: 5 appm N and 2 appm O for single crystal 4H-SiC, 0.1 appm N and 4 appm O for RH SiC, and 0.1 appm N and 10 appm O for CT SiC. The as-fabricated material microstructures have been investigated in the previous study (Koyanagi et al., 2023).

A nuclear grade of SiC/SiC composite consisting of Hi-Nicalon Type-S (HNS) fibres, a pyrolytic carbon (PyC) fibre interphase coating, and a chemical vapour infiltrated (CVI) SiC matrix was studied. The material was fabricated at Rolls-Royce High Temperature Composites Inc. (lot number: 13C-529). The fibre architecture was 2D satin-weave, 0°/90° stacking. The thickness of PyC interphase was around 100 nm. The fibre volume fraction and porosity were ~37% and ~13%, respectively. The representative surface microstructure is presented in Figure 1D. As the specimen is cut from a larger panel, connected porosity is opened from the cut edges. This increases the open surface area compared to the as-manufactured panel where pores would have

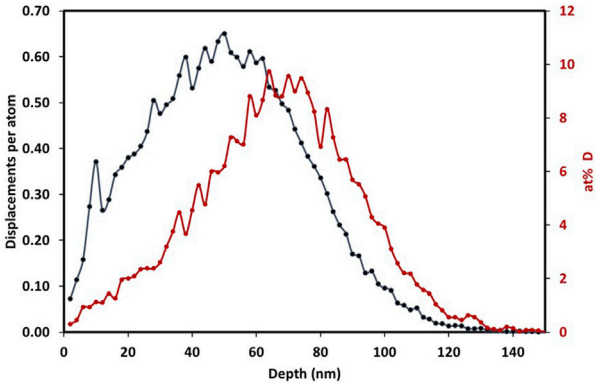

FIGURE 2
SRIM damage and range profiles for 5.46×10^{16} ions/cm^2 5 keV D^+ ion implantation into 3C-SiC with a damage peak of 0.61 dpa and concentration peak of 9.6 at% deuterium.

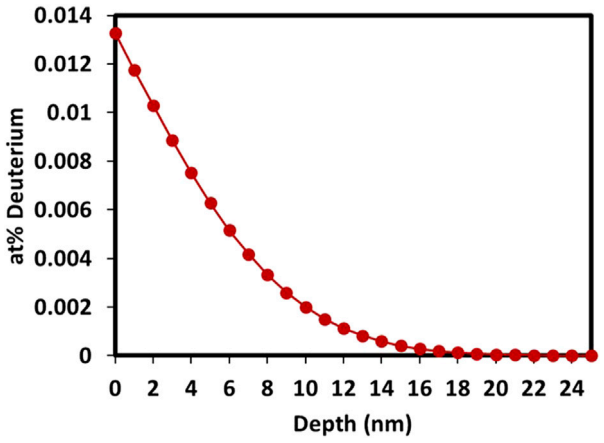

FIGURE 3
Predicted depth profile of deuterium diffused into SiC based on the polycrystal hydrogen isotope diffusivity equation obtained in reference Causey et al. (1993).

been sealed by the chemical vapour deposition process. The 3D porosity or effective surface area of this specimen was not characterised, although further detailed characterisation of this batch of composite material is provided in references (Katoh et al., 2014; Koyanagi and Katoh, 2017).

A neutron irradiated specimen of RH CVD SiC of identical grade to the unirradiated material described above was used to investigate the effects of radiation defects on deuterium retention. This specimen was irradiated in the High Flux Isotope Reactor at ORNL to a nominal fluence of 2.24×10^{25} n/m^2 (E > 0.1 MeV) ~2.24 displacements per atom. Post-irradiation dilatometry measurement of passive SiC thermometry (Campbell et al., 2016) indicated an irradiation temperature of ~950°C. Although the dilatometry method is not practically applied to very high irradiation temperature (>~1,000°C), this study detected subtle recovery of length during annealing (e.g., indication of irradiation temperature). This specimen was chosen as the irradiation temperature is well above the deuterium charging temperature so will minimise defect annealing during gas charging and TDS experiments.

2.2 Deuterium charging, low energy ion implantation, and thermal desorption spectroscopy

Deuterium was introduced to the specimens in two different ways: low energy ion implantation and gas charging by diffusion. Prior to introducing deuterium, all specimens were thermally annealed in vacuum at 900°C with a 10°C/min ramp rate and 1 h dwell time to remove any trapped gaseous species. This is below the irradiation temperature therefore microstructural evolution would not be expected to occur in the irradiated specimen.

One ion implantation experiment was conducted on a unirradiated RH SiC specimen to investigate the effects of ion implantation and gas charging on thermal desorption spectroscopy results. Implantation was at room temperature, with 10 kV accelerating potential on a D_2^+ charged molecule corresponding to 5 keV/D. The fluence of ions was 5.46×10^{16} D/cm^2. SRIM profiles for atomic concentration and displacements per atom are shown in Figure 2 with an implantation range of ~100 nm, 9.6 at% peak concentration, and 0.61 peak dpa (Ziegler et al., 2010). Threshold displacement energies were 21 eV for carbon atoms and 35 eV for silicon atoms in 3C-SiC, density was 3.21 g/cm^3, and the quick Kinchin-Pease method was used (Devanathan and Weber, 2000; Stoller et al., 2013). The beam is focussed into a ~1.5 mm diameter area on the specimen.

Gas charging to diffuse deuterium into specimens was carried out in a single-ended quartz tube within an alumina tube furnace. This quartz tube is solely used for deuterium charging experiments to avoid cross contamination. The tube was evacuated and purged with deuterium gas twice before the experiment began. The sample was heated in 1 atm of deuterium at 450°C and held for 1 hour before cooling. This is below the neutron irradiation temperature therefore microstructural evolution would not be expected to occur. Based on Fick's laws for diffusion from a constant pressure source, and diffusion coefficients calculated by Causey and Wampler for tritium in CVD SiC, a deuterated depth of ~20 nm is predicted, plotted in Figure 3 (Causey and Wampler, 1995; Causey et al., 1993). These diffusion coefficients and activation energies refer to "vapour deposited SiC", similar to the materials used in this work, are commonly referred to in the literature, however the experimental temperature is higher to enable measurable diffusion depths and rates, which may cause different diffusion mechanisms, therefore this diffusion depth should be considered as an estimate only. This depth is a roughly equivalent range to a 500 eV ion implantation, however does not induce displacement damage to SiC. The atomic concentration of deuterium is lower than achieved by high fluence ion implantation but is achieved on the whole specimen surface rather than a focussed area from the ion beam, therefore generating sufficient signal for the mass spectrometer during TDS.

Thermal desorption spectroscopy (TDS) was carried out in the same tube furnace as used for gas charging experiments, but using a separate quartz tube. The single-ended quartz tube containing the sample was connected to a mass spectrometer and evacuated, followed by heating at 10°C/min to 900°C while measuring the

outgassing species. TDS experiments were conducted within 1 hour of the gas charging experiment. Desorption rates were normalised to the surface area of the specimens measured by digital calliper or to the ion beam implanted area, and the mass spectrometer was calibrated using standard gas leaks. Contributions to deuterium desorption rate is only reported for mass 4 corresponding to D_2 molecules as this ensures only the intentionally introduced deuterium release is measured and is not influenced by hydrogen background in the experiment. The composite specimen contains open porosity as seen in Figure 1D and therefore a higher surface area than measured by the sample dimensions. For TDS of the ion implantation experiment, the release rate is normalised to the area of the ion implantation.

2.3 Raman spectroscopy

Raman spectroscopy was carried out on the deuterium ion implanted RH CVD SiC after thermal desorption spectroscopy. Raman mapping was conducted using a Renishaw inVia confocal Raman microscope with a 532 nm wavelength laser focussed through a ×100 objective operated at 30 mW source laser power with a 0.01 s integration time. Spectra were acquired over a 500 × 500 μm area with 2 μm step size covering a portion of the ion implanted and unimplanted region.

2.4 Ab-initio calculations of hydrogen binding and migration energies

Interactions of hydrogen with vacancy defects in silicon carbide were investigated using Density Function Theory (DFT) calculations implemented with Vienna Ab-initio Simulation Package (VASP) (Kresse and Hafner, 1993; Kresse and Furthmüller, 1996a; Kresse and Furthmüller, 1996b). The generalized gradient approximation (GGA-PBEsol) was used for exchange and correlation functional (Perdew et al., 1996) and the acceleration of DFT optimized calculations was achieved by using Projector Augmented Wave (PAW) pseudo-potentials (Blöchl, 1994). The Gamma sampling of k points in the Brillouin zone, with k-mesh spacing of 0.2 $Å^{-1}$, was used to calculate the total energies. The plane-wave cut-off energy value of 750 eV has been employed after carefully checking total energy calculations for both primitive cubic and supercell calculations with the convergency of 10^{-5} eV and the force components were relaxed to 10^{-3} eV/Å. Calculations were performed using the Marconi and Leonardo HPC machines hosted by CINECA, Italy. Formation energies and binding energies were calculated for several situations of hydrogen in defects and interstitial sites, and multiple hydrogen atoms were introduced sequentially to investigate multi-atom trapping. Hydrogen was used for these simulations rather than deuterium. Nudged elastic band calculations were performed to investigate migration barriers along different pathways for interstitial hydrogen in SiC.

Defect formation energy is defined as the energy of the defective system minus the energy of the perfect system minus the sum of the ground state energy of the species added or removed (Equation 1):

$$E_f = E_{total,\ defected} - E_{total,\ perfect} - \sum_i n_i \mu_i \quad (1)$$

where n_i is the number of atoms of species i added (n > 0) or removed (n < 0) and μ_i is the elemental ground state energy per atom.

Enthalpy of solution for interstitial hydrogen atoms is the total energy of the system including interstitial hydrogen minus the total energy of the perfect crystal cell without hydrogen, minus half the energy of an isolated H_2 molecule (Equation 2):

$$E_s = E_{tot,H} - E_{tot,perf} - \frac{1}{2}E_{H_2} \quad (2)$$

Binding energy of a defect cluster A^nB^m which is made up up n defects of type A and m defects of type B is given by Equation 3:

$$E_b = E_{tot,A^nB^m,} - nE_{tot,A} - mE_{tot,B} + (n+m-1)E_{tot,perfect} \quad (3)$$

Where a negative value corresponds to attraction between defects. When extra defects are added to a pre-existing defect cluster, the sequential binding energy is used to calculate the binding energy of the extra defect, for example, the sequential binding energy of adding a H atom (A) into the defect complex with a vacancy (B) interacting with nH can be written as Equation 4:

$$E_{b,seq} = E_{tot,H^{n+1}V,} - E_{tot,H} - E_{tot,H^nV} + E_{tot,perfect} \quad (4)$$

3 Results

Thermal desorption spectroscopy results for different grades of SiC which have been gas charged in identical conditions are shown in Figure 4. The HNS-CVI composite has a far higher release rate than the other specimens due to its higher specific surface area, and has been scaled to one-10th of its release rate in the plot. This specimen has a single broad asymmetric desorption peak with a maximum desorption rate at 590°C. 4H-SiC single crystal has the lowest desorption rate of all the specimens with no distinct peaks, but a broad increase in release rate above 450°C. Both the RH and CT polycrystalline 3C-SiC specimens have broad peaks with high release rates between 550°C and ~850°C. The RH specimen has ~40% higher D_2 release rate than the CT specimen across the temperature range of the D_2 release peak. Although RH and CT specimens have overall similar desorption profile shape, a careful analysis shows a minor difference of their desorption profiles: the RH release rate is approximately constant between 600°C and 700°C before declining, while CT release rate increases until a maximum at 700°C before decreasing, which may indicate different ratio of trap types in RH vs. CT or an additional trapping site in CT that desorb deuterium at high temperature. The RH specimen neutron irradiated at 950°C to 2.24 dpa behaves significantly differently to the pristine RH specimen, showing only a single, sharp desorption rate peak at 550°C before returning to a low D_2 release rate for the remaining temperature range.

Figure 5 shows the TDS results of D_2 release rate from the D_2^+ ion implanted RH specimen. This shows a steadily increasing release rate before a maximum release rate at 850°C. This desorption rate peak is close to the maximum temperature of these TDS experiments but appears to be falling at the time the experiment ended. The

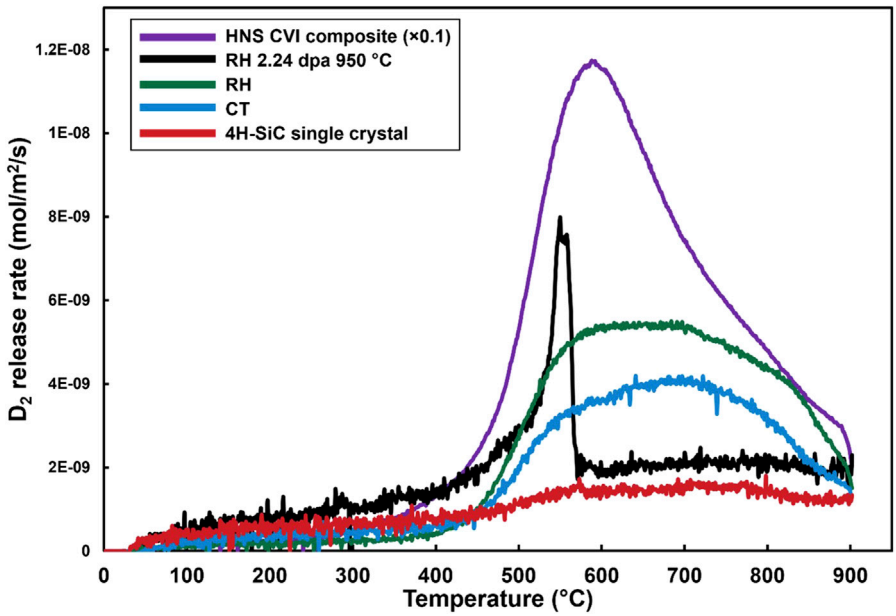

FIGURE 4
Deuterium release rate results for TDS experiments of various microstructures of deuterium gas charging experiments. The line for the HNS CVI composite has been scaled to 1/10th of its release rate for clarity on this scale against the other specimens.

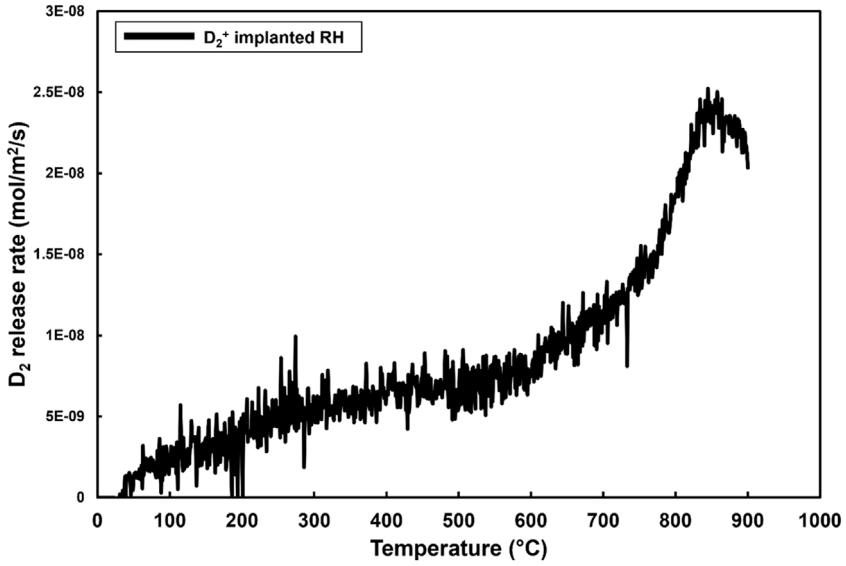

FIGURE 5
Deuterium release rate TDS result from D_2^+ ion implanted RH SiC showing a single peak at 850°C.

microstructure of this specimen is identical to the RH specimen used for the gas charging experiment, but shows a significantly different desorption profile.

Raman spectra comparing pristine non-implanted regions of the RH SiC specimen and the deuterium implanted region following TDS are shown in Figure 6. As the implanted deuterium and displacement damage is within only 120 nm of the specimen surface, the majority of the signal arises from underlying unirradiated material explaining the dominance of the transverse optic (TO) and longitudinal optical (LO) vibrational mode peaks of 3C-SiC in both spectra. However, following implantation and TDS, there appears a peak around 1,400 cm^{-1} which is attributed to mixed sp^2 and sp^3 carbon bonding as observed in amorphous SiC (Chaâbane et al., 2012; Bolse, 1999). The reduction in bond connectivity by forming trigonal sp^2 carbon bonds in addition to tetrahedral sp^3 carbon is a necessary step towards amorphisation (Leide et al., 2019; Bolse, 1999). Annealing up to 900°C did not recover carbon bond disordering due to the long-range stochastic

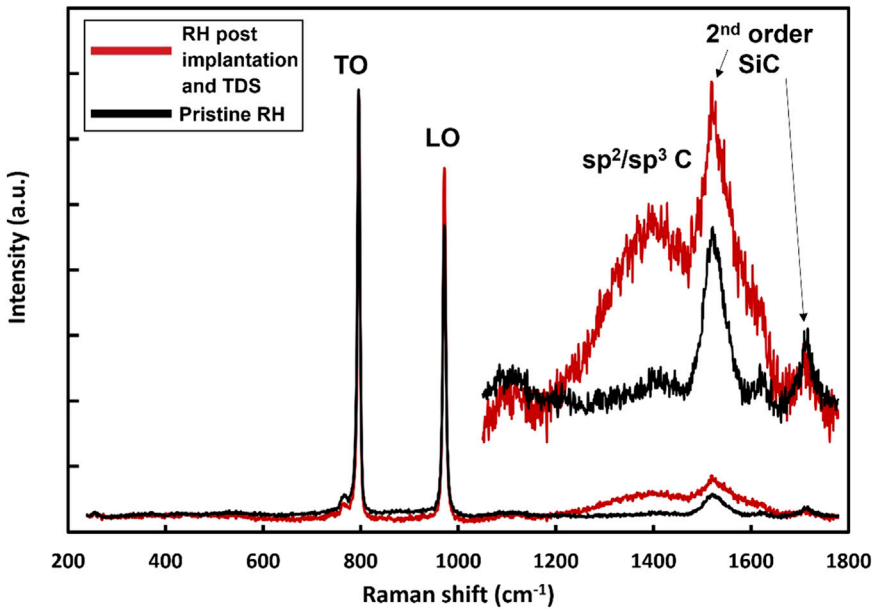

FIGURE 6
Raman spectra of pristine RH 3C-SiC and RH 3C-SiC following deuterium implantation and TDS. The region above 1,050 cm^{-1} is shown on 7× scale. TO, LO and second order SiC peaks are labelled, along with the appearance of a peak around 1,400 cm^{-1} attributed to C-C networks in amorphous SiC.

reconfiguration required to re-form a crystalline structure and the stability of sp^2 carbon bonds in a C-C network.

Key experimental results from this work have been summarised in Table 1 along with literature results from comparable work. This summary table will be discussed in the later Discussion sections and in relation to the following results from first principles calculations.

3.1 Calculations of hydrogen binding energies with vacancies

Formation energies (E_f) or solution energies (E_s) of single hydrogen atoms inserted into various defect sites were calculated, shown in Table 2. This includes substitutional sites, interstitial sites, and interstitial sites with a carbon or silicon vacancy. Hydrogen substitutions onto silicon or carbon lattice sites have very high formation energies E_f and are unfavourable to occur in combination with vacancies in a lattice. It is thermodynamically favourable to maintain the vacant site with the hydrogen atom in an interstitial position denoted by H_{TSi} for a tetrahedral silicon interstitial site, H_{TC} for a tetrahedral carbon interstitial site, and H_{ABc} for the anti-bond centre site which is the opposite vector from a Si-C tetrahedral bond direction. The $H_{TSi}V_C$ defect complex has the lowest formation energy for carbon vacancies, and the $H_{ABc}V_{Si}$ complex is the lowest formation energy defect for silicon vacancies. The silicon vacancies have greater binding energies for hydrogen in all interstitial positions than carbon vacancies indicating that they are stronger trap sites.

Figure 7 plots the charge density difference between a perfect crystal and four hydrogen atoms on anti-bond carbon sites with a silicon vacancy which is surrounded by first nearest neighbour carbon atoms. This shows the localisation of electronic charge between carbon atoms and hydrogen indicating the formation of strong covalent hydrocarbon bonds. The first nearest neighbour carbon atom which is bonding to H has a distorted charge density on the opposite side, and the next nearest carbon atom's charge density is also modified by the presence of hydrogen nearby.

As shown in Figure 8 and Table 3, hydrogen atoms in carbon vacancies have approximately the same sequential binding energies up to 6 hydrogen atoms indicating little geometric dependency. The sequential binding energy of hydrogen atoms in a silicon vacancy remains strong for up to 4 atoms. The fifth atom which is added to the silicon vacancy has an extremely small sequential binding energy, −0.142 eV. This indicates a strong 4-fold geometric dependency, potentially related to the tetrahedral C-H covalent bonding previously identified.

Thermal desorption requires two steps: first de-trapping, then diffusion to a surface to be released. The lowest solution energy interstitial site for hydrogen is calculated to be the H_{ABc} position, at 2.155 eV (Table 2). The migration between H_{ABc} sites has been considered by nudged elastic band calculations. Three distinct pathways for interstitial migration have been identified, and can be described based on Figure 9 and summarised in Table 4. Pathway 1→4 is simply switching symmetric ABc sites on the same carbon atom and has a low energy barrier. This may not necessarily be considered a migration step as the interstitial site is associated with the same atom. To be a true jump, another step is required along pathway 1→5 which is the shortest migration distance but is moving to an ABc site associated with a different carbon atom. Pathway 1→2 is a migration to another ABc site associated to a different carbon atom, but across the plane of silicon atoms and requires a longer distance displacement, but not a significantly higher energy barrier than pathway 1→5.

TABLE 1 Summary of key experimental observations including literature comparisons. dpa for deuterium ion implantations in literature has been calculated using SRIM for comparison.

Specimen	Deuterium loading	TDS profile description	Ref.
RH	Gas charging, 450°C, 1 atm, 1 h	Broad peak between 550°C and 850°C. Constant between 600°C and 700°C before declining rate	This work
	Ion implantation, 10 keV D_2^+, 5.46×10^{16} D/cm^2, room temperature. ~0.66 dpa	Single peak, 850°C	This work
RH irradiated, 2.24 dpa, 950°C	Gas charging, 450°C, 1 atm, 1 h	Single narrow peak at 550°C. Higher release rate than unirradiated	This work
CT	Gas charging, 450°C, 1 atm, 1 h	Lower retention than RH. Broad peak between 550°C and 850°C. Maximum desorption rate at 700°C	This work
4H-single crystal	Gas charging, 450°C, 1 atm, 1 h	Very low broad peak above 450°C	This work
HNS SiC/SiC	Gas charging, 450°C, 1 atm, 1 h	Very high intensity broad peak from 450°C. Maximum at 590°C	This work
β-SiC wafer	Ion implantation, 1 keV D_2^+, 1×10^{18} D/cm^2, (~15 dpa), various temperatures	Room temperature 2 peaks 527°C = Si-D 727°C = C-D Above 500°C single broad higher temperature peak with low intensity	Oya et al. (2005)
CVD SiC, unpolished	Ion implantation, 0.2 keV D_2^+, 1×10^{13} D/cm^2 and 1×10^{18} D/cm^2 (~8 dpa) room temperature	4 peaks 177°C = deuterium adsorbed on surface. 377°C = interstitial deuterium 527°C = Si-D 727°C = C-D	Oya et al. (2013)
β-SiC	Ion implantation, 10 keV D_2^+, 1×10^{18} D/cm^2 (~11.5dpa), room temperature. Various helium implantations	3 peaks 527°C = Si-D 807°C = C-D deuterium in helium pre-implanted carbon-rich regions 927°C = C-D	Sugiyama et al. (2002)
Sintered SiC CVD SiC coated graphite *Plus other materials*	Ion implantation, 1 keV D^+, 1×10^{20} D/cm^2 (1,500 dpa), room temperature *Plus study of energy and temperature*	657°C primary peak with shoulder around 927°C. Same for both SiC samples When implantation temperature is above 427°C, only a small high temperature peak around 900°C exists	Koller et al. (2019)

TABLE 2 Relaxed supercell formation, binding, and solution energies of various hydrogen defect positions in SiC.

Configuration	E_f (eV)	E_b (eV)	E_s (eV)
H_{Si}	8.503		
H_C	5.458		
H_{TSi}			2.805
H_{TC}			3.187
H_{BC}			2.476
H_{ABc}			2.155
$H_{TSi}V_C$	4.234	−2.912	
$H_{ABc}V_C$	4.353	−2.143	
$H_{TC}V_C$	5.261	−2.267	
$H_{ABc}V_{Si}$	6.456	−4.213	
$H_{TC}V_{Si}$	7.502	−4.198	
$H_{TSi}V_{Si}$	8.289	−3.029	

Lowest formation energy defect complexes are highlighted in green.

Binding energies can be incorporated into an effective diffusivity of hydrogen in SiC (D_{eff}) using the McNabb and Foster formula (Equation 5) (Sun et al., 2018; Oriani, 1970).

$$D_{eff} = \frac{D_{perf}}{1 + (c_v)\, exp\left(\frac{E_b^{V-H}}{kT}\right)} \tag{5}$$

D_{perf} is the diffusivity of hydrogen in a perfect crystal, $D_{per} = D_0 \exp(-E_a/kT)$, D_0 is the diffusion coefficient given by $D_0 = a^2\nu 6$ where a is the jump length given in Table 4 for pathway 1→5 with E_a = 0.44 eV ν is a vibrational frequency based on the mass of a deuterium atom (3.32 × 10^{-27} kg) and the diffusion pathway energy and jump length, given by $\nu = \sqrt{(2E_a/ma^2)}$. The vacancy concentration per atom of SiC, c_v, is estimated at 6.27 × 10^{-2}, for the purposes of illustration based on a defect production of ~2.7 vacancies/cm^3/neutron/cm^2 from reference (Bratus, 2015), and the neutron fluence of the irradiated RH sample. Although c_v may be an overestimation of vacancy population as irradiations in (Bratus, 2015) were conducted at room temperature, D_{eff} is relatively insensitive to c_v. Using calculated values, D is plotted against 1,000/T in Figure 10 for

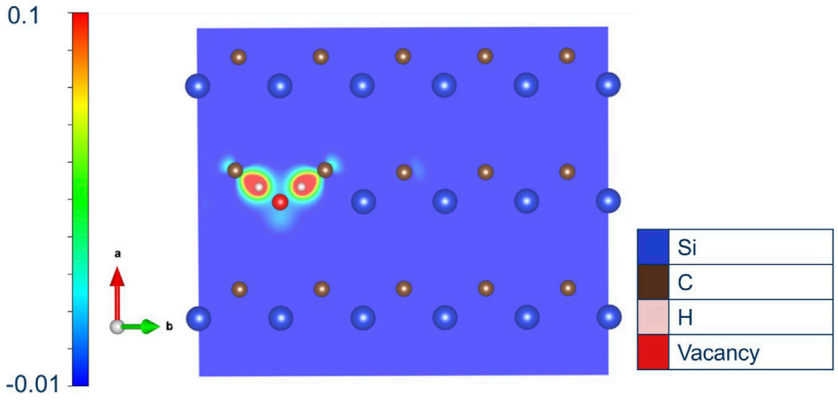

FIGURE 7
Plot of charge density difference relative to a perfect crystal for four hydrogen atoms in a silicon vacancy. Relative localisation of charge density is seen in the direction of carbon atoms.

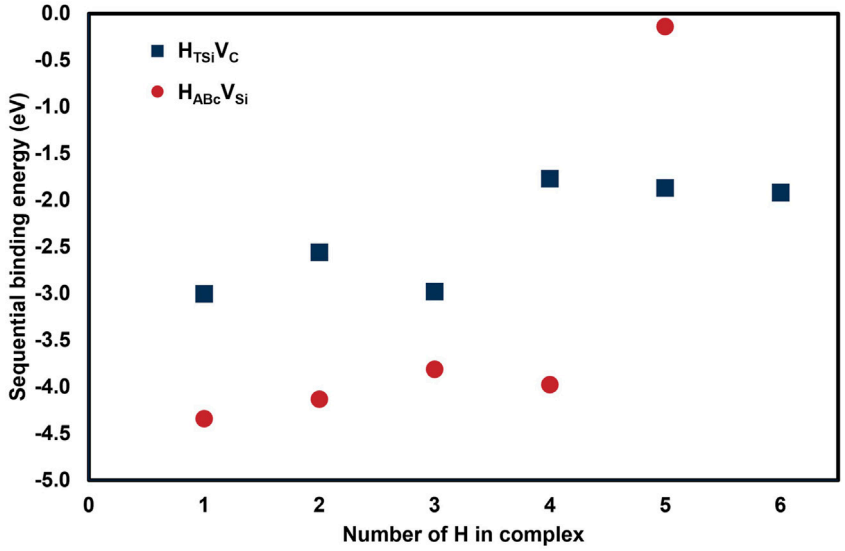

FIGURE 8
Sequential binding energy of multiple hydrogen atoms in carbon or silicon vacancies.

TABLE 3 Sequential binding energies for multiple hydrogen atoms inserted into carbon or silicon vacancies.

Number of inserted H atoms	Sequential binding energy (eV)	
	$H_{TSi}V_C$	$H_{ABc}V_{Si}$
1	−3.00	−4.34
2	−2.56	−4.13
3	−2.98	−3.81
4	−1.77	−3.98
5	−1.87	−0.14
6	−1.92	

a perfect 3C-SiC crystal, a polycrystal D_{poly} based on the diffusion equation from reference (Causey et al., 1993), and 3C-SiC containing carbon or silicon vacancies. $D_{poly} = 9.8 \times 10^{-8} exp(-1.89eV/_{kT})$ m²/s from reference (Causey et al., 1993) and was calculated by fitting predicted release rate curves to experimental isothermal desorption rate data from deuterium/tritium release experiments in the temperature range 1,100°C–1,500°C. Although this is not a perfect comparison to our work, this is considered the most representative polycrystal diffusivity equation to use in this comparison as the grade of material is high purity cubic SiC similar to what has been studied here and the diffusion was calculated based on gas charging rather than ion implantation experiments which gave different results according to the authors in reference (Causey et al., 1993).

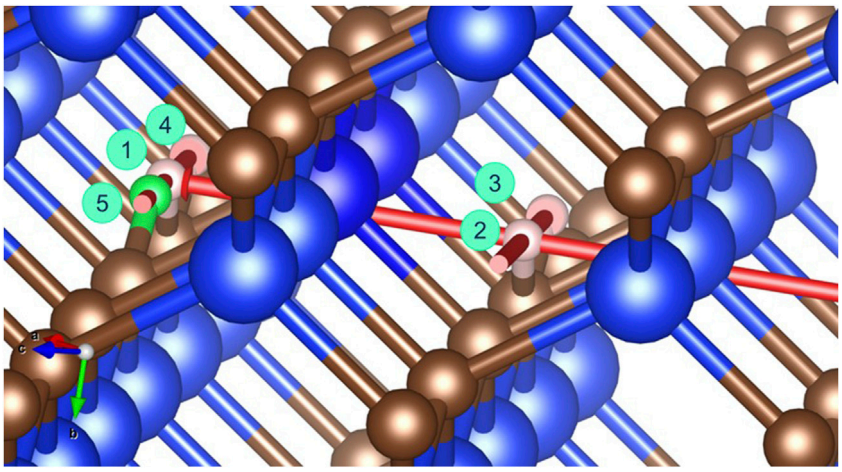

FIGURE 9
Hydrogen interstitial migration pathways between H_{ABc} sites in a SiC crystal. Numbers are related to migration pathways from position 1 described in Table 4 and in the text, 2→3 is equivalent to 1→4. Red arrows indicate pathway directions. Large blue circles represent silicon atoms, medium brown circles represent carbon atoms, and small pink circles represent hydrogen, with position 5 labelled in green as the final position for an interstitial diffusion step from position 1→5.

TABLE 4 Hydrogen interstitial pathways, distances after relaxation, and energy barriers.

Pathway	Distance (Å)	Energy barrier (eV)
1→5	1.22	0.44
1→4	1.86	0.15
1→2	3.08	0.54

Straight lines are fitted to the datapoints in Figure 10 to calculate effective diffusion coefficients and activation energies based on $D = D_{0,eff} \exp(-E_{a,eff}/kT)$, and are given in Table 5. $D_{0,eff}$, is a function of vacancy concentration, c_v, which has been assumed as 6.27×10^{-2} in this work.

In summary, this set of calculations indicates very strong binding of up to 4 hydrogen atoms in a silicon vacancy, and potentially more than 6 hydrogen atoms in a carbon vacancy, but less strongly bound. Effective diffusion coefficients have been calculated for diffusion in a 3C-SiC crystal containing radiation-induced vacancies.

4 Discussion

4.1 Key results

This study has identified key differences in the retention of deuterium in irradiated SiC, and unirradiated SiC of different microstructures. The key experimental TDS results are summarised in Table 1 along with key results from similar samples studied in the literature. The neutron irradiated SiC specimen shows a single peak in deuterium release rate suggesting a specific, dominant type of trapping site, whereas unirradiated specimens of the same material have a broad temperature range of deuterium release. DFT calculations of hydrogen interaction with different vacancies shows stronger binding for hydrogen in a silicon vacancy than in a carbon vacancy, but this strong binding is limited to only 4 hydrogen atoms in the silicon vacancy, whereas carbon vacancies can accommodate at least 6 hydrogen atoms. Although the DFT calculations give insight to binding of hydrogen to vacancies and interstitial sites, the trapping and desorption mechanisms in irradiated SiC still requires further investigation, especially the effects of larger radiation defects than monovacancies.

The microstructure of different grades of high purity 3C SiC has a measurable difference on deuterium retention; the overall higher deuterium retention in the RH specimen than the CT specimen is attributable to larger grain boundary surface area in RH, while the slightly increased desorption at ~700 °C in CT may suggest the contribution from its high stacking fault density. Although there are measurable differences between RH and CT grades, their desorption profiles share similar features related to their broadly similar microstructures, supporting the reproducibility of TDS results across the different samples in this work. Composite specimens with open porosity have very large deuterium release rates with a broad peak potentially related to the larger effective surface area of the composite or free carbon in their microstructure. The specimen where deuterium was introduced by ion implantation has high temperature deuterium release rate peak whereas an identical gas charged specimen has a broad temperature range for deuterium release beginning from lower temperatures. This may suggest a different deuterium trapping mechanism associated with different charging methods or a possible modification of the specimen during ion implantation, especially when viewed in conjunction with the crystal damage observed by Raman spectroscopy. These key results will be discussed in the following sections.

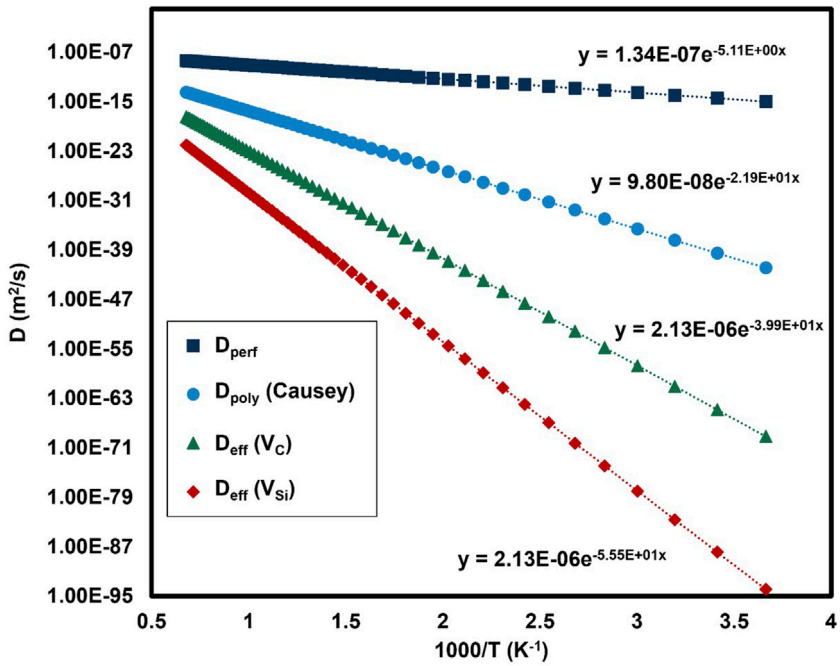

FIGURE 10
Calculated diffusivities of hydrogen in a perfect 3C cubic crystal, a deuterium/tritium diffusivity in a polycrystal from (Causey et al., 1993) and hydrogen diffusivity in 3C SiC containing carbon or silicon vacancies.

TABLE 5 Effective diffusion coefficients for hydrogen in a perfect 3C crystal, containing vacancies, and comparison to experimental polycrystal results for hydrogen isotope diffusivity (Causey et al., 1993).

System	$D_{0,eff}$ (m^2/s)	$E_{a,eff}$ (eV)
D_{perf}	1.34×10^{-7}	0.44
D_{eff} (vC)	2.13×10^{-6}	3.44
D_{eff} (vSi)	2.13×10^{-6}	4.78
D_{poly} (Causey et al., 1993)	9.80×10^{-8}	1.89

4.2 Microstructural effects on hydrogen isotope trapping

The 4H SiC single crystal sample served as a reference with no grain boundaries or microstructural features allowing us to study the fundamental trapping of deuterium in SiC_4 (CSi_4) covalently bonded tetrahedral units. Although a 4H-SiC sample was used due to the difficulty of obtaining free-standing cubic single crystals, the local structure is identical to 3C-SiC (only the intermediate-range and long-range structure are slightly altered), so the retention mechanisms are likely to be similar. The single crystal has a very low retention of deuterium based on its desorption rate, suggesting that SiC either has a very low inherent trapping of deuterium, or release requires more energy than the thermal energy which was introduced in the TDS experiment here. Considering the low intrinsic deuterium retention in pristine single crystal SiC, the retention and subsequent release observed in other pristine specimens must be related to microstructural features.

The two CVD SiC specimens (RH and CT) are high purity monolithic specimens with different microstructure. The characterization of their hydrogen desorption behaviours allows one to evaluate the effect of grain boundaries and stacking faults. The broad desorption rate peak is across the same temperature range for both samples indicating similar retention mechanisms. RH has a higher overall deuterium retention which maybe be related to the overall higher grain boundary area density than the CT sample. Grain boundaries in CVD SiC are mostly high angle boundaries which may enable faster diffusion (Cancino-Trejo et al., 2018). The local chemistry of the grain boundary is likely to be important for retention of hydrogen isotopes as the binding of hydrogen to Si or C terminated surfaces of SiC wafers has different energies during hydrogenation to passivate SiC crystals (Seyller, 2004). Causey et al. proposed that hydrogen isotopes are trapped at grain boundaries by forming covalent bonds to carbon or silicon atoms, lowering the effective diffusivity of hydrogen through a polycrystal of SiC compared to a perfect crystal, which is in agreement with the interstitial diffusivity calculated for a perfect crystal from DFT results in Figure 10 (Causey et al., 1993). Molecular dynamics simulations have shown small angle tilt boundaries are most stable with excess carbon at their core (Jiang et al., 2017), and nanograins sintered in a carbon-rich environment result in a monoplane of carbon along their boundary (Stelmakh et al., 2024). These effects are explained by higher interstitial mobility of carbon than of silicon or vacancy diffusion, and diffusion of carbon interstitials to grain boundaries during high temperature treatments or irradiation (Jiang et al., 2017; Wang X. et al., 2020). Carbon depleted grain boundaries with average 45.8at% C were observed in CVD SiC (supplied by Rohm and Haas and Insaco) using core loss EELS, while the carbon concentration increased following ion irradiation at 300°C (Wang X. et al., 2020). Grain boundaries are a spectrum of angles

and surface terminations (whether Si or C with different energies (Seyller, 2004)), and are likely to be sinks for impurities, which may explain the broad desorption peak. The low temperature limit of this broad peak is above the peak desorption rate temperature for purely Si-D bound deuterium, and below the peak desorption rate temperature for C-D bound deuterium according to the analysis in reference (Oya et al., 2005). As grain boundaries are faster diffusion pathway, during the charging experiment, deuterium is likely to diffuse from the specimen surface along grain boundaries and remain in this plane. The desorption rate is highest at 700°C for the CT sample whereas it is constant between 600°C and 700°C for the RH sample (Figure 4). This may suggest a different ratio of trap types between the CT and RH samples, potentially with a greater fraction of stronger C-D based traps in CT. The high stacking fault density of the CT sample may also contribute to strong trapping and will need further investigation of the energetics of stacking faults.

The composite sample has several orders of magnitude higher desorption rate due to the high surface area, which also relates to a higher absorption rate during the gas charging experiment. Additionally, the composite microstructure differs from the monolithic SiC samples in having a pyrolytic carbon interface between the matrix and fibres, and the fibres which contain free carbon and impurities such as boron. CVI processing also produces a more complex matrix SiC microstructure than CVD, as the gas flow rates, temperatures, and mixtures need to be adjusted to optimise for infiltration between fibres, and deposition rate. This multi-day processing can result in different grain sizes within the specimen, along with oxidation between stages of CVI. A detailed assessment of hydrogen isotope retention in different composite microstructures is beyond the scope of this paper. The effects of this complex microstructure are difficult to deconvolute from the single desorption rate peak maximum at 600°C. The desorption profile from the SiC composite appears to be very similar to that from graphite reported in (Oya et al., 2005) showing the probable dominant effects of free carbon in the composite on deuterium retention. In a fusion reactor component, a dense layer of CVD SiC is likely to be facing the plasma or tritium breeding material so trapping by free carbon should be minimised and the results from the CVD SiC monoliths in this work are most representative. These results for the composite may be representative of a component where matrix cracking has occurred and there are pathways for hydrogen isotopes to reach the internal material structure.

While different microstructures of SiC and SiC composites have been studied, it is difficult to quantitatively compare our results with previous work as microstructures are not provided. While Oya and Sugiyama's work specifies cubic β-SiC, it is not clear if it is single crystal or polycrystal and what the impurities or composition might be (Oya et al., 2013; Sugiyama et al., 2002; Oya et al., 2005; Oya et al., 2002). Sánchez et al. studied reaction bonded SiC with 10% residual silicon and containing metallic impurities which create defects in both the α-SiC and silicon phases (Sánchez et al., 2016). Nobuta et al.'s work uses a liquid phase sintered, hot pressed composite "NITE (nano infiltration transient eutectic)" containing alumina and yttria additives which remain as residual oxide phases in the microstructure (Nobuta et al., 2015; NOBUTA et al., 2011). It is not clear if the samples were implanted on the as-received surface or a polished surface of the composite plate. The surface preparation determines the microstructure which is exposed to the deuterium ion beam and the phases which deuterium will be implanted into. There is also no mention of trapping in residual oxide phases which tend to accumulate on grain boundaries and particularly at triple points (Terrani et al., 2018). Considering the discussion of the importance of SiC grain boundaries for retaining deuterium, the role of grain boundary phases in NITE materials will be important.

The nudged elastic band calculations show very low diffusion activation energies for hydrogen between interstitial sites, only 0.54 eV (Table 4), suggesting easy diffusion of hydrogen isotopes in a SiC matrix. This is in a perfect crystal and does not include microstructural effects nor defects. This is in agreement with other literature, although negatively charged hydrogen shows higher energy barriers (Wang W. et al., 2020). Diffusion coefficients and activation energies found experimentally suggest slower diffusion, indicating microstructural effects are important at hindering the effective diffusion of hydrogen isotopes (Causey and Wampler, 1995; Esteban et al., 2002). Strong binding energies for hydrogen to different vacancy types, in combination with low interstitial migration barriers suggests that diffusion is easy within a perfect SiC crystal, but effective diffusion can be low as hydrogen gets trapped by grain boundaries or other defects. This explains the suitability of SiC as a hydrogen permeation barrier, however may lead to strong retention of hydrogen isotopes (Causey and Wampler, 1995; Henager, 2007).

4.3 Irradiation effects on hydrogen isotope trapping

The single well defined deuterium desorption rate peak at 560°C for the neutron irradiated specimen is at lower temperature than pristine specimens, indicating a different trapping mechanism compared to the pristine samples. As the desorption rate peak is at a lower temperature, less energy is required to detrap deuterium and diffuse it to the surface than in the pristine samples. The temperature for peak desorption rate is close to the peak desorption rate temperature for Si-D bonds proposed in the literature suggesting a change from deuterium trapping associated with carbon atoms to being associated with silicon atoms after irradiation (Oya et al., 2013; Sugiyama et al., 2002). The DFT calculations show smaller binding energy for hydrogen atoms to silicon atoms around a carbon vacancy than to carbon atoms around a silicon vacancy. This agrees with the previous experimental observation that the Si-D desorption rate peak is at a lower temperature than the C-D desorption rate peaks (Oya et al., 2013; Oya et al., 2005).

Although candidates for the deuterium trapping sites in irradiated SiC can be discussed based on the literature data, identification of dominant trapping sites remains a challenge. This is because various radiation defect structures could be formed in irradiated SiC. The irradiation temperature of ~950°C is considered to be within the point defect swelling regime where atomistic interstitial and vacancy type defects cause lattice expansion (e.g., swelling) (Snead et al., 2007). The modelling on point defects in this study is an initial step towards a comprehensive understanding of the interaction of various radiation defects in SiC and hydrogen isotopes but will need to be extended to larger length scales and complexity.

The dominant point defect type for high temperature low dose irradiation is the carbon vacancy which has a high migration energy requiring annealing temperatures above ~1,400°C, whereas carbon and silicon interstitials and silicon vacancies are all mobile below 900°C, lower than the irradiation temperature of the specimen in this work (Roma et al., 2012; Katoh and Snead, 2019). The predicted preference of carbon vacancies, and the associated silicon nearest neighbours supports the interpretation of the 560°C desorption rate peak being associated with Si-D bonding. There is no broad desorption rate peak between 550°C and 850°C which was considered to be attributed to grain boundaries in the pristine sample. This suggests that the effective diffusivity of deuterium in SiC has been further reduced; deuterium diffuses interstitially in the grains until trapped in crystal trapping sites and before reaching a grain boundary. Alternatively, radiation damage may have modified the nature of the SiC grain boundaries as they act as defect sinks during irradiation preventing it acting as a hydrogen trap (Jiang et al., 2017).

The deuterium ion implantation process could have an effect of low temperature ion irradiation, corresponding to 0.6 peak dpa of displacement damage, as shown earlier in Figure 2. Such displacement damage by deuterium implantation is not trivial in SiC, but has not been considered in previous work (Oya et al., 2013; Sugiyama et al., 2002; Nobuta et al., 2015; Koller et al., 2019; Sánchez et al., 2016). The threshold amorphization dose of SiC at room temperature is below 0.5 dpa using light ions (Snead and Zinkle, 1994). A threshold temperature depends on ion species, but is between 300°C and 400°C for heavy ions (Snead and Zinkle, 1996; Kerbiriou et al., 2009). Threshold amorphization doses have been exceeded in almost all deuterium implantation experiments in the literature, however we do not know if these specimens have amorphous islands or complete amorphization. Although some researchers have conducted deuterium implantations above the threshold amorphization temperature, there is still displacement damage in their specimens which has not been characterised and may impact deuterium trapping (Nobuta et al., 2015; Koller et al., 2019; Sánchez et al., 2016). Raman spectroscopy shows signs of C-C bonding even after high temperature annealing during TDS which is evidence of partial amorphisation, and significant structural damage. Below ~150°C there is effectively no mobility for self-interstitials nor vacancies in SiC, and extended structural disordering including homonuclear C-C bonding in trigonal-tetrahedral networks may be expected, including both sp^3 and sp^2 bonding in partially amorphized SiC. Low temperature low dose proton irradiations of SiC have been proven to create stable silicon vacancies surrounded by first nearest neighbour carbon atoms, among other defects (Kawasuso et al., 2005; Itoh et al., 1990).

The single TDS peak at ~850°C in the deuterium ion implanted RH sample corresponds to the C-D trapping in a carbon-rich environment proposed in (Sugiyama et al., 2002), and no peaks corresponding to Si-D are observed. This suggests that C-D bonds are being formed during the restructuring of Si-C covalent tetrahedra into C-C homonuclear bonds in amorphous SiC, and that displacement damage is creating trapping sites during the ion implantation process which are different to those in the gas charged pristine and neutron irradiated specimens. The desorption rate peak is quite sharp and at a higher temperature than the broad desorption rate peak in the pristine specimen. Being at a higher temperature indicates a higher binding energy for deuterium in the ion implanted specimen than in the pristine gas charged specimen, possibly related to trapping in silicon vacancies rather than at grain boundaries. Considering the low migration barrier energy for interstitial diffusion of deuterium, and the high defect density in low temperature ion implantation, implanted deuterium will be trapped locally to a carbon atom within a short diffusion radius and will not diffuse to a grain boundary. This mechanism explains the sharp desorption rate peak from the deuterium ion implanted specimen. In reference (Sugiyama et al., 2002) helium was pre-implanted to study the effects of helium in trapping sites, and displacement damage was also introduced. This helium implantation was done at room temperature where dynamic annealing is minimal and to a dose of 1×10^{18} He/cm^2 corresponding to ~40 peak dpa, almost certainly enough to (partially) amorphize the surface, or at least considerably modify the lattice with significant chemical disordering which explains the increase in their C-D signal allocated to "peak 2" for desorption from carbon-rich SiC. Amorphous SiC necessarily creates trigonal sp2 C-C bonds which may be broken up by preferential bonding with hydrogen, necessitating higher temperatures to release hydrogen. The role of helium atoms on trapping remains unclear. Helium atoms can occupy vacancies, potentially impacting their capacity for trapping hydrogen isotopes in the subsequent deuterium implantation (Kim et al., 2009). Further modelling work is ongoing to evaluate the interaction of helium and other transmutation produces with hydrogen and displacement defects and will be correlated to complementary experiments.

The calculated binding energy of hydrogen in silicon vacancies is stronger than for hydrogen in carbon vacancies, therefore requiring more thermal energy to release. However, for more than 4 atoms in a silicon vacancy, the binding energy for subsequent hydrogen atoms is close to zero, they are effectively untrapped and will migrate to another trapping site in agreement with previous calculations by Sun et al. (Sun et al., 2017). Carbon vacancies continue to trap at least 6 hydrogen atoms; Sun et al. calculate up to 8 atoms are stable in a carbon vacancy (Sun et al., 2017). Considering carbon vacancies have a higher capacity for hydrogen, this may explain the sharp desorption rate peak in a narrow temperature range as hydrogen atoms are mostly bound to these traps. Silicon vacancies can only trap 4 hydrogen atoms before becoming saturated, and C-C homonuclear bonding clusters have limited C-D bonding sites, therefore at higher hydrogen concentrations as used in literature other trap types are observed including Si-D. Calculated effective diffusivities for deuterium in 3C-SiC containing vacancies are significantly lower than both the perfect crystal and polycrystal due to the strong binding of hydrogen in vacancies. This may make SiC a very good hydrogen isotope permeation barrier in an irradiation environment, however retention may be relatively large and hydrogen isotopes will remain in a grain and not necessarily diffuse to grain boundaries. The presence of other transmutation products and more complex defect structures (e.g., vacancy clusters with different size and composition) and their

influence on trapping and effective diffusion requires further investigation.

4.4 Future research opportunities

This paper has identified the importance of microstructure on deuterium trapping in SiC, and the need to further understand the retention in complex engineering composites and trapping by radiation defects produced under different irradiation conditions. Grain boundaries are an important trap for hydrogen isotopes, and also for other radiation defects and other transmutation elements, therefore further characterisation of SiC grain boundaries should be carried out. The chemical environment of radiation defects and grain boundaries, specifically the chemical bonding states of carbon and silicon, should be investigated in more detail to understand the mechanisms of hydrogen isotope trapping in these sites. Deuterium ion implantation has identifiably modified the structure of the material being studied, and this modification needs to be included when interpreting TDS results. Further experiments should be done to study the defects created using deuterium implantation and how these are interacting with the implanted deuterium ions as a function of dose and sample temperature. Studying neutron irradiated samples has advantages for reliably understanding the damage caused to reactor components, however for deuterium retention experiments it poses challenges. Ion implantation may modify the defects in the neutron irradiated sample by creating new defects, while gas charging above the irradiation temperature will anneal radiation defects. This prevents us studying samples which have been irradiated below the deuterium gas charging temperature. During TDS, radiation defects will be annealing as well as deuterium being desorbed–decoupling these effects may be challenging. However, these results will allow us to investigate stability of vacancies containing hydrogen isotopes, and potentially be more representative of a component in a fusion reactor. Neutron irradiation also produces transmutation products which will be significant in high energy fusion neutron irradiations (Sawan et al., 2013; Gilbert et al., 2013). Transmutation in a fission neutron spectrum is orders of magnitude lower and has not been investigated here, however future studies should look at the interaction of hydrogen isotopes with other transmutation products, including the metallic elements which can change the local charge of defects in SiC, which will impact the binding of charged forms of hydrogen (Wang W. et al., 2020). While this work has studied deuterium and hydrogen, tritium is the most concerning hydrogen isotope in the context of a fusion reactor blanket. Atomistic calculations and experimental results indicate that the key characteristic of hydrogen isotope trapping in SiC is chemical, whether to vacancies or grain boundaries; therefore tritium may be expected to behave similarly. Interstitial diffusion of tritium can be predicted based on that of deuterium by considering the isotope effect as in (Wimmer et al., 2008). Classically, the ratio of diffusivity of H:D:T is proportional to the inverse square root of their isotopic mass, however in practice microstructural and material effects on diffusion appear to be more significant than the isotope effect based on a recent literature review (Urrestizala et al., 2023).

5 Conclusion

A variety of as-fabricated SiC microstructures have been investigated for their deuterium retention properties to identify the microstructural features of most interest. The comparative study indicated that grain boundaries are the most important trapping sites in pristine polycrystalline SiC, giving a range of trapping energies and desorption temperatures. Carbon vacancies are discussed to be possibly dominant trapping sites in high temperature neutron irradiated SiC, having a lower binding energy and thermal desorption temperature than pristine SiC. Deuterium ion implantation at room temperature could create radiation defects which potentially include C-C homonuclear bonding structures and silicon vacancies leading to strongly trapped deuterium as C-D bonds. DFT calculations show that hydrogen isotopes in a perfect crystal have low interstitial migration barrier energies so can diffuse easily in undamaged SiC, but DFT calculations of hydrogen interaction with point defects show that vacancies are strong traps. Experimental results indicate that grain boundaries are also strong traps for deuterium. Further work will be required to quantify retention in a variety of conditions and SiC microstructures, and to fundamentally understand the interaction of displacement damage and transmutation products in a fusion environment.

Data availability statement

The raw data supporting the conclusions of this article will be made available by the authors, without undue reservation.

Author contributions

AL: Data curation, Formal Analysis, Investigation, Methodology, Resources, Supervision, Visualization, Writing–original draft, Writing–review and editing. WZ: Conceptualization, Data curation, Formal Analysis, Investigation, Methodology, Resources, Supervision, Validation, Writing–review and editing. IF-V: Data curation, Formal Analysis, Investigation, Methodology, Software, Writing–review and editing. DN-M: Data curation, Formal Analysis, Investigation, Methodology, Project administration, Resources, Supervision, Validation, Writing–review and editing. TK: Conceptualization, Funding acquisition, Investigation, Project administration, Resources, Supervision, Writing–review and editing.

Funding

The author(s) declare that financial support was received for the research, authorship, and/or publication of this article. AJL was supported by the Royal Academy of Engineering under the Research Fellowship programme. This work was partially supported by the US

Department of Energy, Office of Fusion Energy Sciences, Fusion Materials Program and Early Career Research Program under contact DE-AC05-00OR22725 with UT-Battelle LLC. A portion of this research used resources at the HFIR, a DOE Office of Science User Facility operated by ORNL. This work has been part-funded by the EPSRC Energy Programme [grant number EP/W006839/1]. This work has been part-funded by STEP, a UKAEA programme to design and build a prototype fusion energy plant and a path to commercial fusion. DNM and IFV would like to thank EUROfusion support for the use of high-performing computing machines: MARCONI and LEONARDO in Bologna, Italy.

Acknowledgments

DNM, IFV, and AJL thank Tesni Haddon-McMillan for her earlier contribution to the results in Table 1. To obtain further information on the data and models underlying this paper please contact PublicationsManager@ukaea.uk.

Licenses and permissions

Conflict of interest

The authors declare that the research was conducted in the absence of any commercial or financial relationships that could be construed as a potential conflict of interest.

Generative AI statement

The author(s) declare that no Generative AI was used in the creation of this manuscript.

Publisher's note

References

Abrams, T., Bringuier, S., Thomas, D. M., Sinclair, G., Gonderman, S., Holland, L., et al. (2021). Evaluation of silicon carbide as a divertor armor material in DIII-D H-mode discharges. *Nucl. Fusion* 61, 066005. doi:10.1088/1741-4326/abecee

Blöchl, P. E. (1994). Projector augmented-wave method. *Phys. Rev. B* 50, 17953–17979. doi:10.1103/PhysRevB.50.17953

Bolse, W. (1999). Amorphization and recrystallization of covalent tetrahedral networks. *Nucl. Instrum. Methods Phys. Res. Sect. B Beam Interact. Mat. Atoms* 148, 83–92. doi:10.1016/S0168-583X(98)00855-6

Boulle, A., Debelle, A., Wallace, J. B., Bayu Aji, L. B., and Kucheyev, S. O. (2017). The amorphization of 3C-SiC irradiated at moderately elevated temperatures as revealed by X-ray diffraction. *Acta Mater* 140, 250–257. doi:10.1016/j.actamat.2017.08.030

Bratus, V. Y. (2015). Thermal annealing and evolution of defects in neutron-irradiated cubic SiC. *Semicond. Phys. Quantum Electron. Optoelectron.* 18, 403–409. doi:10.15407/spqeo18.04.403

Campbell, A. A., Porter, W. D., Katoh, Y., and Snead, L. L. (2016). Method for analyzing passive silicon carbide thermometry with a continuous dilatometer to determine irradiation temperature. *Nucl. Instrum. Methods Phys. Res. Sect. B Beam Interact. Mat. Atoms* 370, 49–58. doi:10.1016/j.nimb.2016.01.005

Cancino-Trejo, F., López-Honorato, E., Walker, R. C., and Ferrer, R. S. (2018). Grain-boundary type and distribution in silicon carbide coatings and wafers. *J. Nucl. Mat.* 500, 176–183. doi:10.1016/j.jnucmat.2017.12.016

Causey, R. A., and Wampler, W. R. (1995). The use of silicon carbide as a tritium permeation barrier. *J. Nucl. Mat.* 220–222, 823–826. doi:10.1016/0022-3115(94)00623-7

Causey, R. A., Wampler, W. R., Retelle, J. R., and Kaae, J. L. (1993). Tritium migration in vapor-deposited β-silicon carbide. *J. Nucl. Mat.* 203, 196–205. doi:10.1016/0022-3115(93)90376-A

Chaâbane, N., Debelle, A., Sattonnay, G., Trocellier, P., Serruys, Y., Thomé, L., et al. (2012). Investigation of irradiation effects induced by self-ion in 6H-SiC combining RBS/C, Raman and XRD. *Nucl. Instrum. Methods Phys. Res. Sect. B Beam Interact. Mat. Atoms* 286, 108–113. doi:10.1016/j.nimb.2011.11.018

Devanathan, R., and Weber, W. (2000). Displacement energy surface in 3C and 6H SiC. *J. Nucl. Mat.* 278, 258–265. doi:10.1016/S0022-3115(99)00266-4

Dienst, W. (1991). Assessment of silicon carbide as a potential wall protection material for fusion reactors. *Fusion Eng. Des.* 16, 311–316. doi:10.1016/0920-3796(91)90203-3

Esteban, G. A., Perujo, A., Legarda, F., Sedano, L. A., and Riccardi, B. (2002). Deuterium transport in SiCf/SiC composites. *J. Nucl. Mat.* 307–311, 1430–1435. doi:10.1016/S0022-3115(02)01282-5

Federici, G., Boccaccini, L., Cismondi, F., Gasparotto, M., Poitevin, Y., and Ricapito, I. (2019). An overview of the EU breeding blanket design strategy as an integral part of the DEMO design effort. *Fusion Eng. Des.* 141, 30–42. doi:10.1016/j.fusengdes.2019.01.141

Gilbert, M. R., Dudarev, S. L., Nguyen-Manh, D., Zheng, S., Packer, L. W., and Sublet, J. C. (2013). Neutron-induced dpa, transmutations, gas production, and helium embrittlement of fusion materials. *J. Nucl. Mat.* 442, S755–S760. doi:10.1016/j.jnucmat.2013.03.085

Henager, C. H. (2007). Hydrogen permeation barrier coatings. *Mat. Hydrog. Econ.*, 181–190. doi:10.1201/9781420006070.ch8

Itoh, H., Yoshikawa, M., Nashiyama, I., Misawa, S., Okumura, H., and Yoshida, S. (1990). Radiation induced defects in CVD-grown 3C-SiC. *IEEE Trans. Nucl. Sci.* 37, 1732–1738. doi:10.1109/23.101184

Jiang, H., Wang, X., and Szlufarska, I. (2017). The multiple roles of small-angle tilt grain boundaries in annihilating radiation damage in SiC. *Sci. Rep.* 7, 1–10. doi:10.1038/srep42358

Katoh, Y., Koyanagi, T., McDuffee, J. L., Snead, L. L., and Yueh, K. (2018). Dimensional stability and anisotropy of SiC and SiC-based composites in transition swelling regime. *J. Nucl. Mat.* 499, 471–479. doi:10.1016/j.jnucmat.2017.12.009

Katoh, Y., Ozawa, K., Shih, C., Nozawa, T., Shinavski, R. J., Hasegawa, A., et al. (2014). Continuous SiC fiber, CVI SiC matrix composites for nuclear applications: properties and irradiation effects. *J. Nucl. Mat.* 448, 448–476. doi:10.1016/j.jnucmat.2013.06.040

Katoh, Y., and Snead, L. L. (2019). Silicon carbide and its composites for nuclear applications – historical overview. *J. Nucl. Mat.* 526, 151849. doi:10.1016/j.jnucmat.2019.151849

Kawasuso, A., Yoshikawa, M., Itoh, H., Chiba, T., Higuchi, T., Betsuyaku, K., et al. (2005). Electron-positron momentum distributions associated with isolated silicon

vacancies in 3C-SiC. *Phys. Rev. B - Condens. Matter Mat. Phys.* 72, 045204–045206. doi:10.1103/PhysRevB.72.045204

Kerbiriou, X., Costantini, J. M., Sauzay, M., Sorieul, S., Thoḿ, L., Jagielski, J., et al. (2009). Amorphization and dynamic annealing of hexagonal SiC upon heavy-ion irradiation: effects on swelling and mechanical properties. *J. Appl. Phys.* 105. doi:10.1063/1.3103771

Kim, J. H., Kwon, Y. D., Yonathan, P., Hidayat, I., Lee, J. G., Choi, J.-H., et al. (2009). The energetics of helium and hydrogen atoms in β-SiC: an ab initio approach. *J. Mat. Sci.* 44, 1828–1833. doi:10.1007/s10853-008-3180-2

Koller, M. T., Davis, J. W., Goodland, M. E., Abrams, T., Gonderman, S., Herdrich, G., et al. (2019). Deuterium retention in silicon carbide, SiC ceramic matrix composites, and SiC coated graphite. *Nucl. Mat. Energy*. 20, 100704. doi:10.1016/j.nme.2019.100704

Konishi, S., Enoeda, M., Nakamichi, M., Hoshino, T., Ying, A., Sharafat, S., et al. (2017). Functional materials for breeding blankets—status and developments. *Nucl. Fusion* 57, 092014. doi:10.1088/1741-4326/aa7e4e

Koyanagi, T. (2022). Irradiation-induced chemical disordering in ceramics: the case of SiC. *J. Nucl. Mat.* 565, 153766. doi:10.1016/j.jnucmat.2022.153766

Koyanagi, T., and Katoh, Y. (2017). Mechanical properties of SiC composites neutron irradiated under light water reactor relevant temperature and dose conditions. *J. Nucl. Mat.* 494, 46–54. doi:10.1016/j.jnucmat.2017.07.007

Koyanagi, T., Katoh, Y., Nozawa, T., Snead, L. L., Kondo, S., Henager, C. H., et al. (2018). Recent progress in the development of SiC composites for nuclear fusion applications. *J. Nucl. Mat.* 511, 544–555. doi:10.1016/j.jnucmat.2018.06.017

Koyanagi, T., Lee, J. J., Keiser, J. R., Gietl, H., and Katoh, Y. (2023). Corrosion characteristics of monolithic SiC materials in beryllium-bearing molten fluoride salt. *Corros. Sci.* 220, 111301. doi:10.1016/j.corsci.2023.111301

Kresse, G., and Furthmüller, J. (1996a). Efficiency of ab-initio total energy calculations for metals and semiconductors using a plane-wave basis set. *Comput. Mat. Sci.* 6, 15–50. doi:10.1016/0927-0256(96)00008-0

Kresse, G., and Furthmüller, J. (1996b). Efficient iterative schemes for *ab initio* total-energy calculations using a plane-wave basis set. *Phys. Rev. B* 54, 11169–11186. doi:10.1103/PhysRevB.54.11169

Kresse, G., and Hafner, J. (1993). *Ab initio* molecular dynamics for liquid metals. *Phys. Rev. B* 47, 558–561. doi:10.1103/PhysRevB.47.558

Leide, A. J., Hobbs, L. W., Wang, Z., Chen, D., Shao, L., and Li, J. (2019). The role of chemical disorder and structural freedom in radiation-induced amorphization of silicon carbide deduced from electron spectroscopy and *ab initio* simulations. *J. Nucl. Mat.* 514, 299–310. doi:10.1016/j.jnucmat.2018.11.036

Li, J., Porter, L., and Yip, S. (1998). Atomistic modeling of finite-temperature properties of crystalline β-SiC. *J. Nucl. Mat.* 255, 139–152. doi:10.1016/S0022-3115(98)00034-8

Lord, M., Bennett, I., Harrington, C., Cooper, A., Lee-Lane, D., Cureton, A., et al. (2024). Fusing together an outline design for sustained fuelling and tritium self-sufficiency. *Philos. Trans. R. Soc. A Math. Phys. Eng. Sci.* 382, 20230410. doi:10.1098/rsta.2023.0410

Nobuta, Y., Hino, T., Yamauchi, Y., and Nozawa, T. (2015). Deuterium retention properties of SiC/SiC composites as plasma facing materials for fusion reactors after deuterium irradiation at elevated temperatures. *J. Vac. Soc. Jpn.* 58, 173–176. doi:10.3131/jvsj2.58.173

Nobuta, Y., Yamauchi, Y., Hino, T., Cho, H.-J., and Yoon, H.-K. (2011). Hydrogen retention properties of SiC/SiC composites as plasma facing material of fusion reactor. *J. Vac. Soc. Jpn.* 54, 149–151. doi:10.3131/jvsj2.54.149

Oriani, R. A., (1970). The diffusion and trapping of hydrogen in steel, *Acta Metall.* 18 147–157. doi:10.1016/0001-6160(70)90078-7

Oya, Y., Hatano, Y., Hara, M., Matsuyama, M., and Okuno, K. (2013). Retention and desorption behavior of tritium in Si related ceramics. *J. Nucl. Mat.* 438, 22–25. doi:10.1016/j.jnucmat.2013.03.001

Oya, Y., Kawaai, K., Morita, K., Iinuma, K., Okuno, K., Tanaka, S., et al. (2002). Retention and re-emission behavior of hydrogen isotopes in SiC. *Phys. Scr. T.* 103, 81–84. doi:10.1238/physica.topical.103a00081

Oya, Y., Onishi, Y., Okuno, K., and Tanaka, S. (2005). Trapping and detrapping mech of deuterium in SiC.pdf. *Mate. Transa.* 46, 552–556.

Pearson, R., Baus, C., Konishi, S., Mukai, K., D'Angio, A., and Takeda, S. (2022). Overview of kyoto fusioneering's SCYLLA© ("Self-Cooled yuryo lithium-lead advanced") blanket for commercial fusion reactors. *IEEE Trans. Plasma Sci.* 50, 4406–4412. doi:10.1109/TPS.2022.3211410

Perdew, J. P., Burke, K., and Ernzerhof, M. (1996). Generalized gradient approximation made simple. *Phys. Rev. Lett.* 77, 3865–3868. doi:10.1103/PhysRevLett.77.3865

Roma, G., Bruneval, F., Ting, L. A., Bedoya Martínez, O. N., and Crocombette, J. P. (2012). Formation and migration energy of native defects in silicon carbide from first principles: an overview. *Defect Diffus. Forum* 323–325, 11–18. doi:10.4028/www.scientific.net/DDF.323-325.11

Sánchez, F. J., Moroño, A., Malo, M., and Hodgson, E. R. (2016). Trapping and thermal diffusion for energetic deuterium implanted into SiC. *Nucl. Mat. Energy*. 9, 383–387. doi:10.1016/j.nme.2016.03.007

Sawan, M. E., Katoh, Y., and Snead, L. L. (2013). Transmutation of silicon carbide in fusion nuclear environment. *J. Nucl. Mat.* 442, S370–S375. doi:10.1016/j.jnucmat.2012.11.018

Sawan, M. E., Snead, L., and Zinkle, S. (2003). Radiation damage parameters for SiC/SiC composite structure in fusion nuclear environment. *Fusion Sci. Technol.* 44, 150–154. doi:10.13182/FST03-A325

Schwarz-Selinger, T. (2023). A critical review of experiments on deuterium retention in displacement-damaged tungsten as function of damaging dose. *Mat. Res. Express*. 10, 102002. doi:10.1088/2053-1591/acfdf8

Seyller, T. (2004). Passivation of hexagonal SiC surfaces by hydrogen termination. *J. Phys. Condens. Matter*. 16, S1755–S1782. doi:10.1088/0953-8984/16/17/016

Snead, L. L., Nozawa, T., Katoh, Y., Byun, T.-S., Kondo, S., and Petti, D. A. (2007). Handbook of SiC properties for fuel performance modeling. *J. Nucl. Mat.* 371, 329–377. doi:10.1016/j.jnucmat.2007.05.016

Snead, L. L., and Zinkle, S. J. (1994). Amorphization and the effect of implanted ions in sic. *MRS Proc.* 373, 377. doi:10.1557/PROC-373-377

Snead, L. L., and Zinkle, S. J. (1996). Threshold irradiation dose for amorphization of silicon carbide. *MRS Proc.* 439, 595. doi:10.1557/PROC-439-595

Stelmakh, S., Gierlotka, S., Skrobas, K., and Palosz, B. (2024). Formation of grain boundaries in nanocrystalline SiC ceramics examined by powder diffraction supported by MD simulations. *J. Alloys Compd.* 978, 173474. doi:10.1016/j.jallcom.2024.173474

Stoller, R. E., Toloczko, M. B., Was, G. S., Certain, A. G., Dwaraknath, S., and Garner, F. A. (2013). On the use of SRIM for computing radiation damage exposure. *Nucl. Instrum. Methods Phys. Res. Sect. B Beam Interact. Mat. Atoms* 310, 75–80. doi:10.1016/j.nimb.2013.05.008

Sugiyama, T., Morimoto, Y., Iguchi, K., Okuno, K., Miyamoto, M., Iwakiri, H., et al. (2002). Effects of helium irradiation on chemical behavior of energetic deuterium in SiC. *J. Nucl. Mat.* 307–311, 1080–1083. doi:10.1016/S0022-3115(02)01048-6

Sun, J., Li, B. S., You, Y. W., Hou, J, Xu, Y., Liu, C. S., et al. (2018). The stability of vacancy clusters and their effect on helium behaviors in 3C-SiC, *J. Nucl. Mat.* 503 271–278. doi:10.1016/j.jnucmat.2018.03.010

Sun, J., You, Y. W., Hou, J., Li, X., Li, B. S., Liu, C. S., et al. (2017). The effect of irradiation-induced point defects on energetics and kinetics of hydrogen in 3C-SiC in a fusion environment. *Nucl. Fusion* 57, 066031. doi:10.1088/1741-4326/aa6b82

Tanabe, T. (2011). Tritium handling issues in fusion reactor materials. *J. Nucl. Mat.* 417, 545–550. doi:10.1016/j.jnucmat.2010.12.112

Terrani, K. A., Ang, C., Snead, L. L., and Katoh, Y. (2018). Irradiation stability and thermo-mechanical properties of NITE-SiC irradiated to 10 dpa. *J. Nucl. Mat.* 499, 242–247. doi:10.1016/j.jnucmat.2017.11.040

Tillack, M. S., Bringuier, S. A., Holmes, I., Holland, L., Santos-Novais, F., and Maldonado, G. I. (2022). GAMBL – a dual-cooled fusion blanket using SiC-based structures. *Fusion Eng. Des.* 180, 113155. doi:10.1016/j.fusengdes.2022.113155

Urrestizala, M., Azkurreta, J., Alegría, N., and Peñalva, I. (2023). Isotope effect of hydrogen and deuterium permeability and diffusivity in fusion reactor materials. A literature review. *Fusion Eng. Des.* 194, 113915. doi:10.1016/j.fusengdes.2023.113915

Wang, W., Li, C., Shang, S. L., Cao, J., Liu, Z. K., Wang, Y., et al. (2020b). Diffusion of hydrogen isotopes in 3C-SiC in HTR-PM: a first-principles study. *Prog. Nucl. Energy*. 119, 103181. doi:10.1016/j.pnucene.2019.103181

Wang, X., Zhang, H., Baba, T., Jiang, H., Liu, C., Guan, Y., et al. (2020a). Radiation-induced segregation in a ceramic. *Nat. Mat.* 19, 992–998. doi:10.1038/s41563-020-0683-y

Widdowson, A., Coad, J. P., Zayachuk, Y., Jepu, I., Alves, E., Catarino, N., et al. (2021). Evaluation of tritium retention in plasma facing components during JET tritium operations. *Phys. Scr.* 96, 124075. doi:10.1088/1402-4896/ac3b30

Wimmer, E., Wolf, W., Sticht, J., Saxe, P., Geller, C. B., Najafabadi, R., et al. (2008). Temperature-dependent diffusion coefficients from *ab initio* computations: hydrogen, deuterium, and tritium in nickel. *Phys. Rev. B - Condens. Matter Mat. Phys.* 77, 134305–134312. doi:10.1103/PhysRevB.77.134305

Yuan, X., and Hobbs, L. W. (2002). Modeling chemical and topological disorder in irradiation-amorphized silicon carbide. *Nucl. Instrum. Methods Phys. Res. Sect. B Beam Interact. Mat. Atoms* 191, 74–82. doi:10.1016/S0168-583X(02)00516-5

Ziegler, J. F., Ziegler, M. D., and Biersack, J. P. (2010). SRIM - the stopping and range of ions in matter. *Nucl. Instrum. Methods Phys. Res. Sect. B Beam Interact. Mat. Atoms* 268, 1818–1823. doi:10.1016/j.nimb.2010.02.091